Thermal performance analysis of thermocline combined sensible-latent heat storage system using cascaded-layered PCM designs for medium temperature applications

Article *in* Renewable Energy · June 2020

DOI: 10.1016/j.renene.2020.01.073

CITATIONS
0

READS
17

4 authors, including:

Naveed Ahmed
Xi'an Jiaotong University
11 PUBLICATIONS **58** CITATIONS
SEE PROFILE

K. E. Elfeky
Xi'an Jiaotong University
17 PUBLICATIONS **130** CITATIONS
SEE PROFILE

Renewable Energy 152 (2020) 684–697

Contents lists available at ScienceDirect

Renewable Energy

journal homepage: www.elsevier.com/locate/renene

Thermal performance analysis of thermocline combined sensible-latent heat storage system using cascaded-layered PCM designs for medium temperature applications

N. Ahmed [a], K.E. Elfeky [a], Lin Lu [b], Q.W. Wang [a, *]

[a] Key Laboratory of Thermo-Fluid Science and Engineering, MOE, Xi'an Jiaotong University, Xi'an, Shaanxi, 710049, China
[b] Department of Building Services Engineering, The Hong Kong Polytechnic University, Hung Hom, Kowloon, Hong Kong, China

ARTICLE INFO

Article history:
Received 21 March 2019
Received in revised form
8 December 2019
Accepted 17 January 2020
Available online 22 January 2020

Keywords:
Thermal energy storage
Thermocline tank
Multilayered PCM
Sensible-latent combination
Cascaded-layered PCM

ABSTRACT

One tank type thermocline thermal energy storage (TES) concept is considered as a possible cost optimized solution for the medium temperature industrial applications, e.g., chemical processing, beverages industry etc. However, one of the drawbacks of this TES configuration is higher thermocline degradation at the end of discharging cycles and overall decrease in performance. In current work a new type of combined sensible-latent heat configuration is introduced to counter these issues. The concept of the proposed thermal storage configuration is to use structured sensible heat cheap material with the space between them occupied by encapsulated phase change material (PCM) capsules, forming cascaded layered packed bed along the tank height and the heat transfer fluid flows between them. A comprehensive unsteady numerical model is formulated based on two-phase Schumann model equations to evaluate performance of the each proposed prototypes. The numerical simulations are performed to investigate the effect of combined sensible rod structure and multi-layered PCMs designs on thermocline temperature profiles, exergy outputs, total thermal energy storage, efficiency in the use of total storage capacity, utilization ratio and the proportion of PCM effectively changing phase. The comparative analysis is performed for four different configurations, i.e., single layered sensible rod with PCM (SLSPCM) arrangement and the three cascaded layered sensible rod with PCM (CLSPCM) arrangements. The overall results show that the TES with a volume fraction arrangement of (40%-20%–40%) is performance wise the best configuration followed by (25%-50%–25%) and (10%-80%–10%), respectively. And SLSPCM is the lowest in the row. The analysis presented in the current study shows that the use of multistage PCMs having suitable combination of layer thickness and fusion temperature together with the inclusion of cheaper structured filler material, offer an efficient and cost effective TES alternative.

1. Introduction

There is an urgent need to make current energy supply and demand scenario economically, environmentally and socially more sustainable [1]. To recover maximum wasted energy from the industrial waste heat recovery processes [2] and to harness the maximum potential of solar thermal energy [3]; are considered as vital alternate energy resources. However, the erratic nature of these potential energy resources hinder the development of an innovative and cost effective TES system capable to overcome the mismatch between seasonal energy supply and demand [4]. One tank type thermocline TES systems are 20–37% more cost effective than two tank type thermal storage units depending on the type of application [5]. TES systems can generally be divided into two types based on mechanical assistance for heat transfer; active TES system and passive TES system. In active TES types usually forced convection mode of heat exchange occurs between the storage material and the heat transfer fluid. Whereas, in passive types the heat transfer mechanism is governed by natural convection or buoyancy driven forces. In these TES units during the charging cycles heat energy is stored by raising the internal temperature of storage material as the HTF is pumped into the tank from top. This heat energy is recovered during discharging by pumping cold HTF from the bottom of TES tank. During charge/discharge cycles the thermal gradient formed between high heated energy regions and low

* Corresponding author.
E-mail address: wangqw@mail.xjtu.edu.cn (Q.W. Wang).

https://doi.org/10.1016/j.renene.2020.01.073
0960-1481/

Nomenclature

T	temperature, K
$T_{HTF,out}$	temperature of HTF at outlet, K
T_i	initial temperature of storage filler, K
T_{mp}	melting point, K
k	thermal conductivity, W/mK
L_{PCM}	latent heat of melting, J/kg
H_{PCM}	enthalpy of PCM, J/kg
u	superficial velocity, m/s
t_c	cutoff time, s
h_0	overall heat transfer coefficient, W/m^2 K
h_v	volumetric heat transfer coefficient, W/m^3 K
G	mass flow rate per unit cross section, kg/m^2 s
A_{SRS}	surface area of SRS in a control volume of length Δx, m^2
A_{PCM}	surface area of PCM capsule in a control volume of length Δx, m^2
Δx	size of control volume, m
ΔP	pressure drop, Pa
Nu	Nusselt number
Pr	Prandtl number
Re	Reynolds number
$Ex_{sup,c}$	overall exergy supplied during charging, J
$Ex_{rec,d}$	overall exergy recovered during discharging, J
E_{SRS}	energy retained by sensible rod structure, J
E_{PCM}	energy retained by PCM, J
E_{HTF}	energy retained by HTF, J
f_{SRS}	fractions of energy accumulated in SRS, %
f_{PCM}	fractions of energy accumulated in PCM, %
E_{pump}	pumping work, J
$E_{pump,c}$	pumping work during charging, J
$E_{pump,d}$	pumping work during discharging, J
$E_{overall}$	overall input energy, J
E_{rec}	energy recovered during discharging, J
$E_{Max.st}$	maximum potential stored energy, J
U.R	utilization ratio

Greek Characters

μ	viscosity, kg/m s
ε	porosity
ρ	density, kg/m^3
η	efficiency, %
η_c	charging efficiency, %
η_{dis}	discharging efficiency, %
$\eta_{overall}$	overall efficiency, %
ψ_{ex}	exergy efficiency, %
σ	capacity ratio
γ	liquid fraction of PCM

Subscripts

HTF	heat transfer fluid
SRS	sensible rod structure
PCM	phase change material
Amb	Ambient

heated energy regions in a single storage tank is called thermocline. The filler material inside tank helps to maintain thermal gradient defining the thickness of thermocline region [6]. Flueckiger et al. [7] presented a very useful review of the various experimental and numerical studies on thermocline storage tanks. The technical analysis and economic feasibility to meet any scale of thermal power unit is primarily based on the integration of TES technologies using sensible heat or latent heat filler material [8].

Sensible and latent heat TES systems have both advantages and limitations. Sensible heat TES systems are easily available well developed technology and use low cost cheap naturally occurring filler materials like concrete, rocks etc. [9]. However, it exhibits the limitations of low storage capacity per unit volume and quick temperature drops at the end of discharging cycles [3]. Whereas, latent heat TES system is comparatively more attractive because of its high storage density with small temperature swings and isothermal features during charging/discharging periods [10]. However, the disadvantages i.e., low thermal conductivity, higher capacity cost per kWh, unstable thermo-physical properties and reduced heat exchange rates during thermal recovery cycles caused by the developing solidification layer; hinder its applicability on commercial scale [11]. The researchers experimentally investigated different mixtures of mannitol and galactitol to come up with a potential PCM candidate for the use in medium temperature TES applications [12]. The same kind of study was conducted by Singh et al. to numerically analyze the melting process in an optimized finned latent heat TES system [13]. The both studies proposed that D-Mannitol is a suitable candidate for the medium temperature TES applications.

In the previous studies, majority of the research works focused on either low temperature (lower than 373 K) TES systems using PCM e.g., parfinn wax [14,15] or high temperature (greater than 773 K) using storage materials such as inorganic salts, ceramics, metallic alloys etc. [9,16]. There is a gap to further explore the potential of TES for medium temperature applications [11]. An investigation conducted by Flueckiger et al. [17] concluded that the overall thermal performance is not improved significantly when the sensible filler material is replaced with latent heat storage material. This issue is tackled by using multistage layers of PCM with increasing melting points from bottom of tank to the top. But this is achieved at the expanse of complicated design and higher storage material costs [18].The effect of fill ratio of the encapsulated PCM layers on thermocline TES using cascaded arrangement of PCMs was examined by Zhao et al. [19]. Aldoss et al. [18] used PCM capsules of paraffin wax with different thermal properties and showed that by increasing the number of multiple PCMs stages, the rate of charge/discharge process is improved with enhanced heat transfer rate and higher capacity ratio. Elfeky et al. [20] presented comparative energy analysis of single and multistage PCM thermocline TES units by using numerical simulations. They concluded that during charge and discharge cycles, the overall efficiency of the three-stage PCMs configuration is higher than that of the single PCM configuration.

The literature review shows that limited studies have been carried out to investigate the hybrid effect of combined sensible-latent heat storage material on thermocline characteristics. Majority of these studies used packed bed filler as storage material which later on experiences the issue of thermal ratcheting [21]. The researchers [22] proposed structured design of the sensible heat storage media, as it has the advantage to avoid thermal ratcheting and for a given volume more thermal energy can be accommodated even at higher temperatures [23]. N. Ahmed et al. [24] investigated the thermocline behavior of combined sensible-latent heat storage tank and presented a parametric analysis showing the effect of porosity variation, inlet velocity and feature size on the discharging performance of the TES system. Zanganeh et al. [25] used 1D

numerical model for sensible and latent heat sections of the thermocline storage tank with separate equations for fluid and filler material. They studied the effect of PCM placed on the top of packed bed. It was concluded that choosing a suitable combination of melting temperature and heat of fusion help to stabilize fluid outlet temperature around its melting point, but it has no significant effect on its efficiency. Galione et al. [26] used energy conservation equations to numerically investigate multilayered solid PCM concept using different design configurations. The analysis concluded that the multilayered solid PCM concept is a promising alternative for thermal storage systems.

In our previous work [27,28], comparative thermo-economic analysis of the proposed configuration concluded that combined sensible-latent heat TES prototype is performance wise and economically more optimized solution than the pure sensible or pure latent heat TES configurations. However, more investigation is needed to explore the correct usage of PCM together with sensible structured material to enjoy the maximum potential of hybrid TES configuration. To the best of authors' knowledge, no work was found for one tank thermocline TES configuration using the concept of structured storage material filled with multi-layered PCM capsules having different melting points for medium temperature applications. The main focus of the current work is to enhance thermal performance of storage tank by proposing a new type of combined sensible-latent heat TES configuration, which is filled with reduced amount of cascaded PCM capsules together with the inclusion of sensible heat cheaper structured storage material.

2. Model formulation

In the current numerical model, the geometric configuration of TES consists of sensible rod structures (SRS) positioned vertically along the tank height with gaps between the structured rods as shown in Fig. 1. Encapsulated PCM capsules with a uniform porosity value occupy the spaces between SRS. The tank has distributors at the end sections to make sure that during charge/discharge the fluid is distributed uniformly in radial direction. The formulation of numerical model is performed for sensible and latent heat sections of TES tank by coupling with the conditions of HTF at their interfaces. Four types of TES configurations are investigated with design arrangements as shown in Fig. 2. The single layered sensible rod with PCM (SLSPCM) configuration contains only one type of D-mannitol PCM capsules between SRS. In cascaded layered sensible rod with PCM (CLSPCM), the melting point of different PCM layers decreases from top to bottom along the tank height. The main idea behind cascaded-layered design arrangements is the proper placement of high to low melting point PCM capsules between SRS. These latent heat filler materials form three stages to maximize the capacity ratio and energy/exergy utilization.

In CLSPCM there are three types of cascaded designs of PCMs having three different kinds of phase change materials PCM-1, PCM-2 and PCM-3. These PCMs exhibit different melting points as mentioned in Table 1 along with their thermophysical properties. The PCMs are selected based on the criterion favoring thermocline behavior of TES units during charge/discharge process. PCM-1 placed on the top in cascaded layer arrangement has the melting point greater than discharging threshold temperature of 448 K. The melting point of middle PCM-2 lies between the discharging threshold and charging threshold temperatures i.e., 438 K. Whereas, the melting point of bottom PCM-3 is less than the charging threshold of 430K. These three PCMs are chosen based on the series of DSC investigations carried out by the authors [12,13] using different mixtures of Galactitol and Mannitol as a potential candidate for medium temperature TES applications. The design

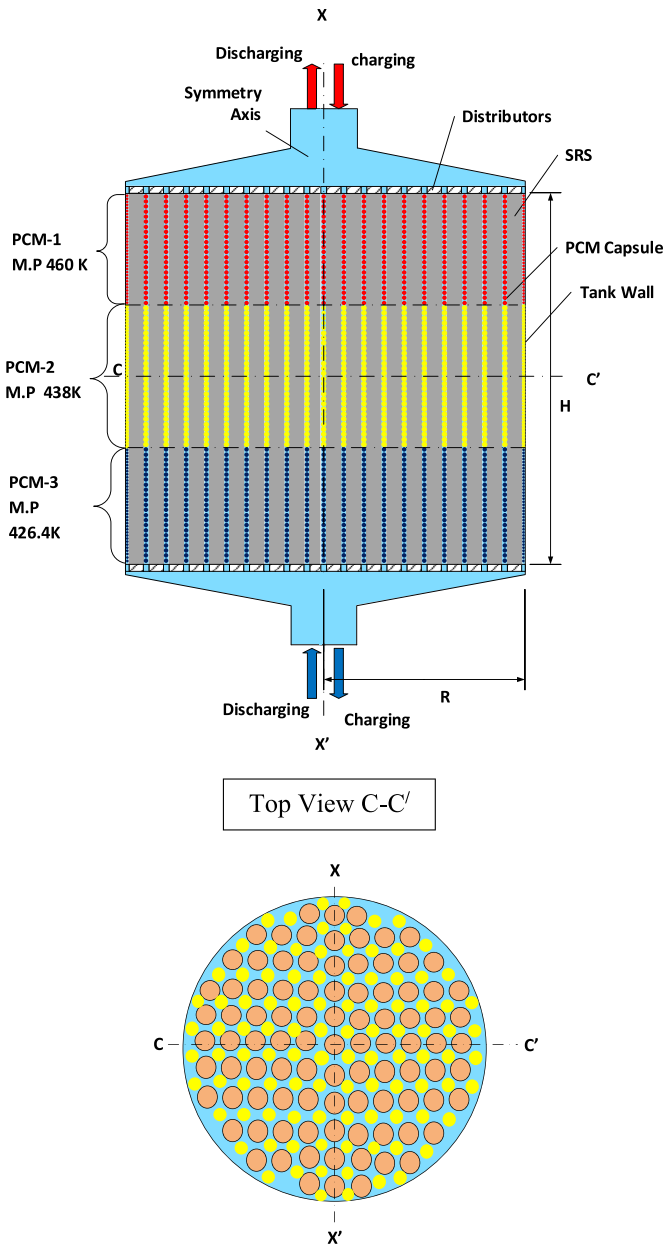

Fig. 1. Sketch of the cascaded layered proposed configuration. PCM-1, PCM-2 and PCM-3 have melting point decreasing from high to low, respectively.

arrangements of PCM capsules for the considered four TES prototypes are shown in Table 2. In cascaded arrangement of PCM capsules, Galactitol is placed as the top PCM-1, D-Mannitol as middle layer PCM-2 and an eutectic mixture of Mannitol and Galactitol in molar ratio of 70:30 is used as the bottom layer PCM-3.

The most relevant assumptions for a differential control volume of height Δx along the tank are:

1. Axisymmetric computational domain is considered with incompressible fluid flow.
2. Negligible conduction in fluid along the axial direction.
3. Uniform distribution of fluid flow and solid storage material in radial direction.
4. Negligible radiation heat transfers and inter particle heat conduction in PCM capsules.

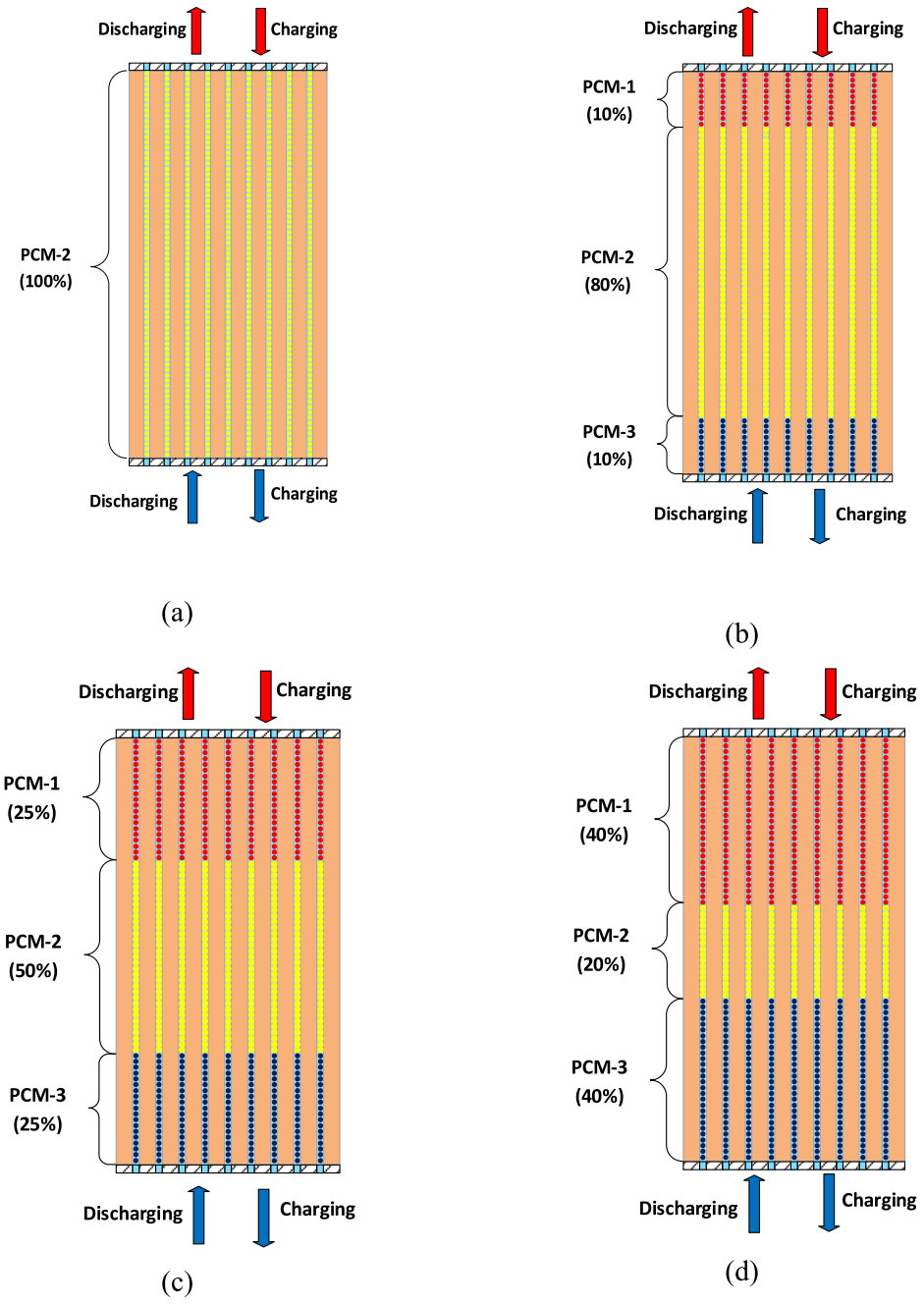

Fig. 2. Sketch of PCM arrangement along the tank height between SRS for different configurations (a) SLSPCM (b) CLSPCM-1 (c) CLSPCM-2 (d) CLSPCM-3.

5. The adiabatic boundary condition is used for the well-insulated storage tank, thus no thermal losses from the tank walls to the surroundings.
6. No gradient of variables in the radial direction is present. This is justified a one-dimensional model.

Table 1
Properties of PCMs [12,29–32].

Property	PCM-1	PCM-2	PCM-3
Melting point (K)	460	438	426.4
Heat of fusion (J/kg)	3.54×10^{05}	3.006×10^{05}	2.92×10^{05}
Specific heat of liquid PCM (J/kg K)	3500	1310	1095
Specific heat of solid PCM (J/kg K)	3395	1200	1010
Density (kg/m^3)	1470	1520	1390
Thermal conductivity of PCM (W/m K)	0.4	0.29	0.35

Table 2
Design arrangements of PCM capsules for the considered configurations.

Configuration	Arrangement of PCM capsules
SLSPCM	100% (D-Mannitol)
CLSPCM-1	10% (Galactitol) + 80% (D-Mannitol) + 10% (Eutectic Mixture of mannitol and galactitol in molar ratio of 70:30)
CLSPCM-2	25% (Galactitol) +50% (D-Mannitol) +25% (Eutectic Mixture of mannitol and galactitol in molar ratio of 70:30)
CLSPCM-3	40% (Galactitol) + 20% (D-Mannitol) + 40% (Eutectic Mixture of mannitol and galactitol in molar ratio of 70:30)

2.1. Governing equations

Based on the considered assumptions, the numerical model is reduced to unsteady axisymmetric problem with separate equations for HTF, sensible heat structured material and multilayered PCMs, respectively. The fluid flow is considered as laminar, Newtonian incompressible with its thermos-physical properties taken as constant over the range of temperature. Accordingly, the general system of governing equations for the developed numerical model can be written as follows.

a. For fluid

The formulated energy balance equation for the fluid flowing with a superficial velocity u entering at a temperature T_{in} in control volume ($A\ \Delta x$) and the internal storage material having an initial temperature of T_i is written as [33].

$$\frac{\partial}{\partial t}(A_{HTF}\ \Delta X \rho_{HTF}\ \varepsilon T_{HTF}) + \nabla.(\rho_{HTF}\ u A_{HTF}\ \Delta X\ T_{HTF}) = \frac{h_{v,SRS}\ A_{SRS}\ \Delta X}{C_{p,HTF}}(T_{SRS} - T_{HTF}) + S_1 \quad (1)$$

where

$$S_1 = \frac{\partial}{\partial t}\left(\frac{\rho_{PCM} A_{PCM} \Delta X\ H_{PCM}(1-\varepsilon)}{C_{p,HTF}}\right) \quad (2)$$

where S_1 is an additional transient term added to account for the enthalpy change of PCM which is caused due to heat exchange with HTF.

b. For sensible heat solid material

Similarly, the energy conservation equation for sensible heat solid storage material is governed by

$$\frac{\partial}{\partial t}(\rho_{SRS}\ \ C_{p,SRS}\ A_{HTF}\ \Delta X\ T_{SRS}(1-\varepsilon)) = h_{v,SRS}\ A_{SRS}\ \Delta X(T_{HTF} - T_{SRS}) \quad (3)$$

The interstitial volumetric heat transfer coefficient h_v, governs the heat exchanged by fluid with the filler material inside storage tank. It is a calculated from overall heat transfer coefficient h_0 of the storage bed. Heat transfer coefficient is evaluated separately for encapsulated PCM capsules and sensible rod structure using the correlations [34].

$$h_v = \frac{6h_0(1-\varepsilon)}{D} \quad (4)$$

Thermal resistance is created by the fluid due to convection on exterior surfaces of PCM capsules and solid rod structure. It is a function of thermo-physical properties of fluid, bed porosity and Reynolds number. The correlation suggested by Wakao et al. is used to calculate the Nusset number [35].

$$Nu = 2 + 1.1\left(6(1-\varepsilon)^{0.6}\right)\mathrm{Re}^{0.6}\mathrm{Pr}^{1/3} \quad (5)$$

where Re, the Reynolds number and Pr, the Prandtl number are calculated using the following correlations

$$\mathrm{Re} = \frac{\rho u D}{\mu};\qquad \mathrm{Pr} = \frac{\mu C_p}{K} \quad (6)$$

c. For PCM storage material

Enthalpy method is used to study phase change phenomenon in PCM capsules caused due to heat exchange with HTF and is governed by the equation [36].

$$\frac{\partial}{\partial t}(\rho_{PCM}(1-\varepsilon)H_{PCM}) = h_{v,PCM}(T_{HTF} - T_{PCM}) \quad (7)$$

where the enthalpy value H_{PCM}, is a function of temperature T_{PCM} and is evaluated depending on the region in which it lies during melting or solidification process. Following three sub-states define the temperature range of phase change phenomenon for the encapsulated PCM:

$$H_{PCM} = \begin{cases} C_{ps,PCM} T_{PCM} & T_{PCM} \le T_{solidus} \\ C_{ps,PCM} T_{PCM} + \dfrac{L_{PCM}}{\left(T_{liquidus} - T_{solidus}\right)}(T_{PCM} - T_{solidus}) & T_{liquidus} > T_{PCM} > T_{solidus} \\ C_{ps,PCM}(T_{mp} - T_i) + C_{pl,PCM}\left(T_{final} - T_{mp}\right) + L_{PCM} & T_{PCM} \ge T_{liquidus} \end{cases} \quad (8)$$

The enthalpy equation for latent heat storage material is used to evaluate the temperature of phase change material with enthalpy being dependent variable and temperature as an independent variable.

The pressure drop in TES unit is estimated using the following relation [37].

$$\Delta P = \frac{2(1-\varepsilon)HG^2}{\mathrm{r}\ \varepsilon^3 \rho}\left(1.75 + 300\frac{\mu}{\mathrm{G\ r}}\right) \quad (9)$$

The fractions of energy accumulated in SRS, f_{SRS} and PCM, f_{PCM} relative to the total thermal energy stored in the thermocline tank are evaluated using the following relations [25].

$$f_{PCM} = \frac{E_{PCM}}{E_{SRS} + E_{PCM} + E_{HTF}} \quad (10)$$

$$f_{SRS} = \frac{E_{SRS}}{E_{PCM} + E_{SRS} + E_{HTF}} \quad (11)$$

where E_{PCM}, E_{HTF} and E_{SRS} are the heat energy retained by PCM, HTF and SRS filler, respectively. Note that the HTF confined within the storage tank contributes with an extra sensible heat energy to the overall storage capacity.

In order to evaluate the energy extraction potential of the proposed TES unit, the overall exergy balance of HTF is evaluated using exergy efficiency (ψ_{ex}). It is defined as the ratio of overall exergy recovered during the discharging cycle ($Ex_{rec,d}$) to the overall exergy supplied during charging cycle ($Ex_{rec,c}$).

$$\psi_{ex} = \frac{Ex_{\mathrm{rec,d}}}{Ex_{\mathrm{sup,c}}} \tag{12}$$

where

$$Ex_{\mathrm{rec,d}} = \int_{t_{0,d}}^{t_{\mathrm{final,d}}} \dot{m}_{\mathrm{HTF}}\, c_{\mathrm{p,HTF}} \left(T_{\mathrm{HTF,out}} - T_{\mathrm{HTF,inlet}} - T_{\mathrm{amb}} \ln \frac{T_{\mathrm{HTF,out}}}{T_{\mathrm{HTF,inlet}}} \right) dt \tag{13}$$

$$Ex_{\mathrm{sup,c}} = \int_{t_{0,c}}^{t_{\mathrm{final,c}}} \dot{m}_{\mathrm{HTF}}\, c_{\mathrm{p,HTF}} \left(T_{\mathrm{HTF,out}} - T_{\mathrm{HTF,inlet}} - T_{\mathrm{amb}} \ln \frac{T_{\mathrm{HTF,out}}}{T_{\mathrm{HTF,inlet}}} \right) dt \tag{14}$$

It results into exergy flow quantity which is the difference between the exergy entering and leaving the storage tank with the HTF.

The charging efficiency is defined as the ratio of the fraction of thermal energy stored in filler material (SRS and PCM) at the end of the charge cycle (E_{stored}) to the summation of overall input ($E_{overall}$) and pumping work ($E_{pump,c}$) [38]:

$$\eta_{\mathrm{C}} = \frac{E_{\mathrm{stored}}}{E_{\mathrm{overall}} + E_{\mathrm{pump,C}}} \tag{15}$$

Discharge efficiency is defined as the ratio of amount of recovered energy (E_{rec}) to the summation of initial stored energy and pumping work ($E_{pump,d}$):

$$\eta_{\mathrm{d}} = \frac{E_{\mathrm{rec}}}{E_{\mathrm{stored}} + E_{\mathrm{pump,d}}} \tag{16}$$

The overall cycle efficiency is defined as the ratio of the energy extracted from the TES tank for a single charge/discharge cycle to the summation of energy stored and pumping energy required [38].

$$\eta_{Overall} = \frac{E_{\mathrm{rec}}}{E_{\mathrm{stored}} + E_{\mathrm{pump,c}} + E_{\mathrm{pump,d}}} \tag{17}$$

where the energy required to pump the HTF is evaluated by the relation [38].

$$E_{\mathrm{pump}} = \int_{0}^{t_d} \frac{A \Delta p\, G}{\rho_{\mathrm{HTF}}} dt \tag{18}$$

During the numerical simulations, charge/discharge operational time is not fixed but it depends on the threshold temperature value of fluid coming out of the proposed TES system.

The utilization ratio is calculated by using the ratio of amount of thermal energy that is extracted during discharge process to the maximum potential of energy storage that could be recovered if the storage materials were to be cooled to the initial temperature [39].

$$\mathrm{U.R} = \frac{E_d}{E_{Max.st}} \tag{19}$$

where the amount of discharged thermal energy is calculated by evaluating the difference between energy that is stored at the end of the charge process to the energy retained by the storage filler at the end of discharge period:

$$E_d = E_{stored,c} - E_{stored,d} \tag{20}$$

The capacity ratio characterizes the amount of thermal energy stored during the charge process as compared to the theoretical maximum thermal energy that can be stored when the temperature of storage material is in equilibrium with the fluid inlet temperature.

$$\sigma = \frac{E_d}{E_{Max.st}} \tag{21}$$

2.2. Initial and boundary conditions

The numerical model is solved with the following set of initial and boundary conditions:

(i) At t = 0

$$\begin{cases} T_{\mathrm{i}} = T_{\mathrm{HTF}} = T_{\mathrm{SRS}} = T_{\mathrm{PCM}} = 405\ K & \text{charging} \\ T_{\mathrm{i}} = T_{\mathrm{HTF}} = T_{\mathrm{SRS}} = T_{\mathrm{PCM}} = 498\ K & \text{discharging} \end{cases} \tag{22}$$

(ii) At inlet section for t > 0

$$\begin{cases} T_{\mathrm{HTF}} = 498\ \mathrm{K}, u = 0.0015\ \mathrm{m/s} & \text{charging} \\ T_{\mathrm{HTF}} = 405\ \mathrm{K}, u = 0.0015\ \mathrm{m/s} & \text{Discharging} \end{cases} \tag{23}$$

(iii) At symmetry axis:

$$\frac{dT_{\mathrm{HTF}}}{dy} = 0,\ \frac{du}{dy} = \frac{dv}{dy} = 0 \tag{24}$$

(iv) At outer wall:

$$\frac{dT_{\mathrm{HTF}}}{dy} = 0,\ \frac{dT_{\mathrm{PCM}}}{dy} = 0,\ \frac{dT_{\mathrm{SRS}}}{dy} = 0,\ u = v = 0 \tag{25}$$

(v) At outlet of storage tank:

$$\frac{dT_{\mathrm{HTF}}}{dx} = 0,\ \frac{dT_{\mathrm{PCM}}}{dx} = 0,\ \frac{dT_{\mathrm{SRS}}}{dx} = 0,\ P = 0 \tag{26}$$

2.3. Numerical modeling

A comprehensive transient numerical model is formulated to evaluate the performance indices of the four different types of hybrid TES configurations and the geometric parameters are shown in Table 3. The computational domain of TES tank has a height of 6 m and radius of 2.5 m. It has a porosity value of 0.5 with filler material distributed radially uniform for the all considered TES configurations. The structured rod and PCM capsules have the radius of 0.03 m and 0.01 m respectively. The formulated one dimensional numerical model is implemented by using energy balance equations as User Defined Scalar (UDS) transport equations in FLUENT software. SIMPLE scheme is used with second order implicit scheme for the transient formulation of temporal terms. Spatial discretization is performed which uses Least Square Cell

Table 3
Geometric parameters with material properties of SRS and HTF.

Parameter	Value
Tank height (H), m	6.0
Tank radius (R), m	2.5
Porosity (ε)	0.5
Density of brick manganese (ρ_{SRS}), kg/m^3	3000
Conductivity of brick manganese (K_{SRS}), W/m K	5.07
Specific heat of brick manganese ($C_{p,SRS}$), J/kg K	1130
Density of HTF (ρ_{HTF}), kg/m^3	940
Conductivity of HTF (K_{HTF}), W/m K	0.10
Specific heat of HTF ($C_{p,HTF}$), J/kg K	2000
Viscosity of HTF (μ_{HTF}), kg/m s	4.90×10^{-04}
Threshold Temperature of HTF during charging (T_{hc}), K	430
Threshold Temperature of HTF during discharging (T_{hd}), K	448

based method with first order upwind schemes. The numerical simulations use quadrilateral dominant mesh grid. The numerical solutions converge when residuals for the UDS and flow variables approach values less than 10^{-6} and 10^{-3}, respectively. This methodology is adopted to account for the performance evaluation of combined sensible-latent heat TES system due to the variation in melting temperature and layer thickness of PCM capsules. The numerical simulations are carried out to address the concerns of quick thermocline degradation during charging/discharging cycles and maximize total energy/exergy utilization while stabilizing the fluid outlet temperature.

In order to verify the accuracy of the developed numerical model, it is necessary to ensure that the results are independent of the grid size. In the current study a grid independence test is performed which validates that the results obtained from the numerical simulations are independent of the mesh size. Four different grid sizes are employed in the current study while keeping the constant time step of 0.3 s. The grid sizes are G-1 = 0.0025 m (finer), G-2 = 0.005 m (fine), G-3 = 0.0075 m (coarse), G-4 = 0.01 m (coarser). Fig. 3 shows the variation in PCM capsule temperature at the center of storage tank (x = H/2) and fluid temperature at the outlet for different grid sizes during charging process. There is a great divergence of temperature in PCM capsules if the coarser grid size of 0.01 m is used. However, it is clear from the presented results that the calculation accuracy of the numerical solutions cannot be further improved by using more refined grid size than 0.0075 m. Hence, in order to maintain the calculation accuracy and save computational time, the mesh size of 0.0075 m is selected for further numerical simulations of the TES systems.

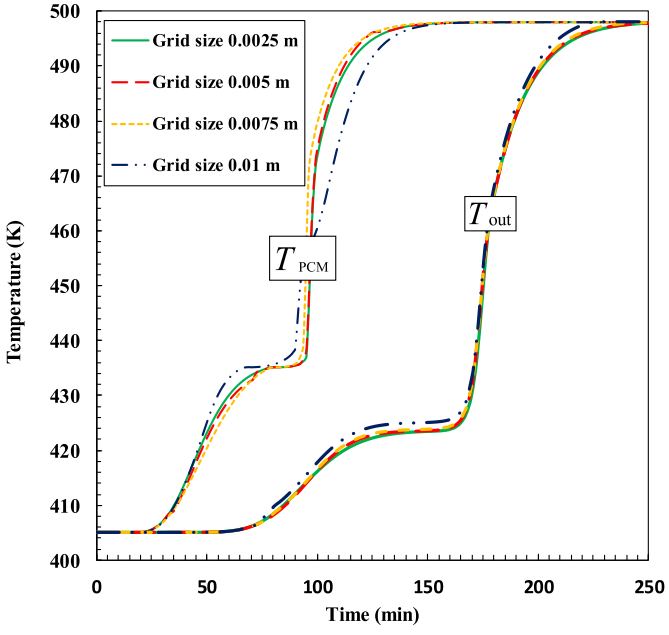

Fig. 3. Temperature of PCM capsule and HTF at the outlet as function of time at different grid sizes.

2.4. Model validation

The formulated numerical model is validated separately for sensible and latent heat storage sections. The numerical model for sensible heat storage section is validated by comparing the simulation results with the experimental data reported by Kuravi et al. [40]. The laboratory-scale TES prototype unit varied the temperature of HTF between 300 °C to 600 °C and large sized bricks are used as storage material. The numerically evaluated and the experimentally measured temperatures of HTF at different axial locations along the tank height at a mass flow rate of 0.0447 kg/s is shown in Fig. 4a. The temperature profiles of fluid are evaluated with in the storage tank at the coordinate points of (0.09, 0.28575) and (0.8, 0.28575). The comparison of numerical results and experimental data shows a maximum and mean deviation of 7.86% and 5.43% respectively, which confirms the validity of the current model, The developed numerical model for latent heat storage material is validated using the experimental results of pilot scale TES prototype reported by the researchers [15] in which they used PCM capsules filled with Praffin Wax and water as HTF. Fig. 4b shows PCM temperature profiles at different locations of the tank during continuous charging cycles with constant inlet fluid temperature of 373 K for a mass flow rate of 2 l/min. These temperature profiles are analyzed in the storage tank at the coordinate points of (0.09, 0.28575) and (0.8, 0.28575). The predicted results present a reasonable trend as stated in experimental measurements with a maximum and mean error of 8.17% and 4.5%, respectively. However, a little inconsistency between the experimental and numerically evaluated results may be attributed to the reasons that the conductivity of capsule shell thickness is not considered in the current work but it is included in the experimental study. It is also because of the simplification of the model neglecting inlet effects of HTF at the entry and the difference in real thermo-physical properties. An overall agreement of the numerically evaluated results with the experimental data confirms validity of the numerical model, forming foundation for the comparative simulation study which is presented and discussed in the next section.

3. Results and discussion

In the current study the melting point is chosen intelligently for the cascaded layered PCMs i.e., decreasing the melting point from top to bottom and choosing the fusion temperature within admissible range to the charge/discharge threshold temperatures. It helps to achieve an enhanced utilization of the whole storage capacity. To use the proposed TES system for an arbitrary medium temperature application, the outlet temperature of fluid during discharging process is limited by the minimum threshold temperature of 448K. This temperature is admissible for the fluid feeding to the specific process. Similarly, the charging process is controlled by the threshold temperature of 430K for the bottom PCM capsules making sure maximum utilization of the whole storage capacity. Therefore, charging/discharging cycle time and the amount of stored energy are evaluated by the level of temperatures attained by fluid at the outlet within admissible temperature range. A thermal buffering effect is created by the layer of PCM capsules positioned at the end sections of the storage tank between rod

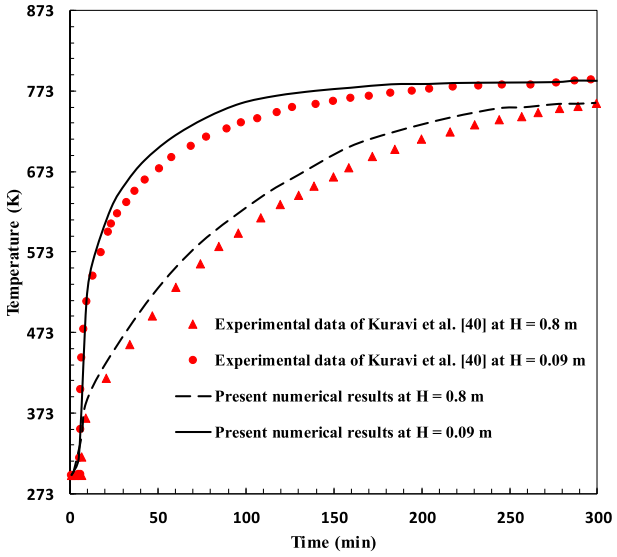

(a)

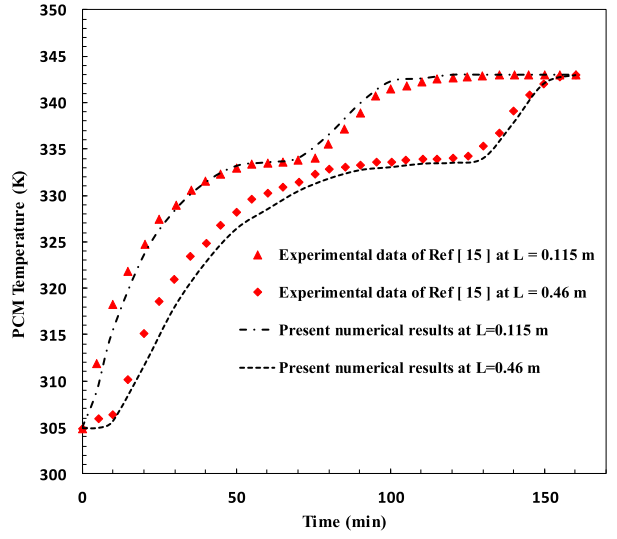

(b)

Fig. 4. Model validation using comparison between numerical results and experimental data for (a) Sensible heat storage section (b) Latent heat storage section.

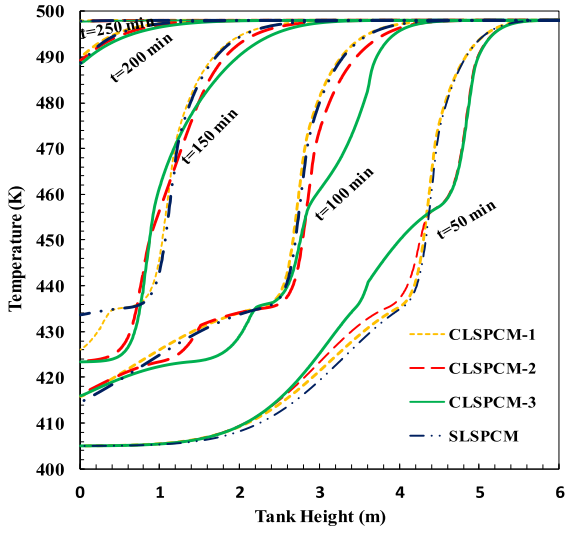

(a)

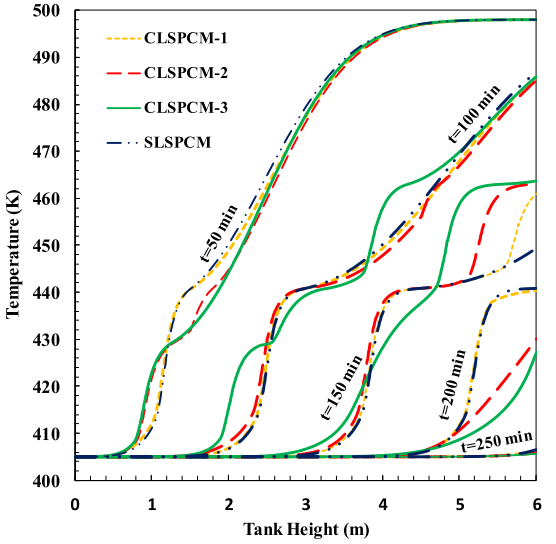

(b)

Fig. 5. Distribution of temperature profiles along tank height at different instants during (a) charging (b) discharging.

structure and it helps to keep the temperature of fluid close to its melting point. This helps to stabilize the fluid outlet temperature while the remaining storage material is charged or discharged with sensible heat energy. Meanwhile the main objective is the evaluation of thermocline performance of single storage tank using different cascaded layer designs of PCM with variable thicknesses and hybridized with sensible heat material in the context of medium temperature applications.

3.1. Temperature profiles in TES systems

The thermocline temperature profiles of HTF inside tank at different instants for the four different prototypes are plotted in Fig. 5. The phase transition state of the PCM capsules when it is between the solidus temperature and liquidus temperature is represented by an interface called pinch point interface. The pinch point interface collapse or break down when the PCM has completely melted. During the charge process as can be seen (Fig. 5a) at t = 50 min for the SLSPCM and CLSPCM-1, the pinch point interface in top layer has stretched into the PCM-2 layer, while a portion of the top PCM-1 capsules for CLSPCM-3 are still in the phase change process. Simultaneously after a charging period of 100 min, the PCMs in top layer of CLSPCM-2 and CLSPCM-3 are completely in molten state; causing the breakdown of pinch point interface with PCM-2 layer. This is because higher thickness of top PCM-1 layers (1.5 m and 2.4 m for CLSPCM-2 and CLSPCM-3 respectively) require more melting heat and longer time. After these instants, the high heated HTF in the respective designed configurations is free to propagate at increased velocity through the storage tank. It is observed that in the final cycles of charge process, more than three quarters of the filler material in the CLSPCM and SLSPCM case has achieved the hot inlet temperature. This is because the higher percentage volume i.e., 40% of the top PCM-1 capsules having high melting point of 460 K takes longer time to

breakdown pinch point interface. Moreover, during the charging process for a low melting point PCMs, the higher difference in temperature between the PCM melting point and the hot inlet fluid stimulates a bigger driving force for heat transfer. This promotes quick progression of the PCM interface. However, when the melting point is high along with greater percentage thickness of PCM as in the top PCM-1 layer for the CLSPCM-3 design; the movement of pinch point interface is slowed down limiting the growth of hot region. Since CLSPCM-1 contains lesser volume fraction of the high melting point PCM-1(10%) as compared to the other CLSPCM designs, it finishes the phase transition process earlier during the initial charge cycles. This result into the breakdown of pinch point interface more swiftly. Similarly, it is true for SLSPCM design as there is no fraction of high melting point PCM-3 and it contains only single layered PCM-2 with low heat of fusion as compared to PCM-3. For the same location from the inlet of storage tank, this design reaches the pinch point interface relatively quickly.

The same reasoning can be used to explain the solidification process in PCM along the tank height and fluid temperature profiles during discharging process. Fig. 5b shows that the pinch point interface at the bottom PCM-3 has stretched up to the top PCM-1 capsules, while a portion of the upper PCM is still in the phase transition process. The lower solidification point of the PCM-3 capsules at the bottom section of storage tank causes the interface point move upward slowly and thus limiting the progression of cold region. The comparative results show that the lower volume fraction of high solidifying PCM-3 capsules for CLSPCM-1 at the bottom induces the completion of solidification process quicker than that of CLSPCM-2 and CLSPCM3, respectively. Moreover, during the discharging process, the initially fully charged hot tank reaches the outlet threshold temperature when the part of PCM-1 capsules placed near the outlet section under goes phase change i.e., starts solidifying. The position of phase changing capsules inside the storage tank can be identified by the location where there is a steep thermal gradient ranging from 435 K to 440.8 K for SLPCM and this for the final state of effective discharge time is located at about 4.1m from the bottom. Therefore, the subsequent discharge process shows that only some part of the available latent energy is exploited in SLPCM design. Moreover, the sensible heat capacity of both the PCM and HTF is much less harnessed than the that of SRS which will be explained in coming results.

Fig. 6 shows the comparative temporal variation of fluid temperature profiles along the tank height at x = H/2 for SLSPCM, CLSPCM-1, CLSPCM-2 and CLSPCM-3 during charge and discharge process. It is observed that during the charging process an increased rate of heat transfer occurs at the pinch point of PCM interfaces and the fluid exits through the interface at a temperature around the phase change temperature. All the considered TES configurations contain layer of PCM-2 at the center of storage tank with a melting point of 438 K but the layer thickness is different in each design arrangement as explained in section 2. It can be seen that during charging process the longest phase transition period for CLSPCM-3 from solid to liquid is 15 min followed by CLSPCM-2 with 9 min. Whereas, CLSPCM-1 and SLSPCM take almost the same phase change duration of 7 min. This is because higher volume fraction of high melting point PCM-1 capsules placed at the upper part of storage tank takes longer time to melt, resulting into low exergy fluid flow for the incoming PCM capsules. Whereas, during discharging process apparently the temperature profile of HTF around the center of PCM-2 in case of CLSPCM-3 shows lower thermocline characteristics as compared to the other configurations. It means that variation of fluid temperature profiles at the center of tank are at lower values for CLSPCM-3 but in the preceding sections it will be at higher value as will be discussed in coming results. This happens due to smallest volume fraction of

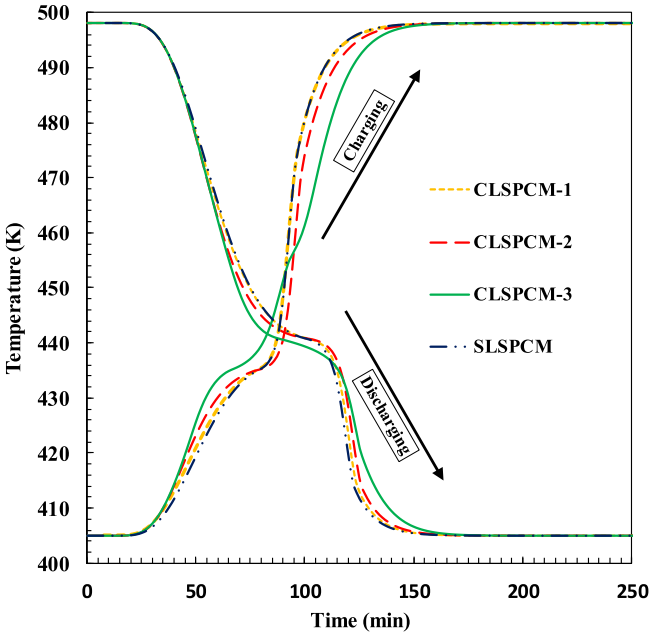

Fig. 6. Variation of temperature profiles at x = H/2 as a function of time during charge and discharge process.

PCM-2 of 20% as compared to 50%, 80% and 100% exhibited by CLSPCM-2, CLSPCM-1 and SLSPCM, respectively. This is also because the increased melting point of PCM-3 and PCM-2 layers from bottom to upper part of TES tank, take the advantage of incoming high exergy fluid flow. It help to accelerate phase transition process at the pinch point interfaces of PCM-2 capsules. This results in to enhanced utilization of latent heat energy as well as extraction of sensible heat from SRS.

The comparison of fluid temperature profiles for the considered four design configurations at the outlet section of storage tank during charge/discharge process as a function of time are shown in Fig. 7. The slope of curve can be used to predict rate of heat exchanged between HTF and the filler material i.e., SRS and PCM. The steeper the slope of curve, the greater the rate of heat transfer and the quicker will be charge/discharge process. Fig. 7a shows that during the charging process, CLSPCM-3 takes longer time to charge but the higher fusion heat value for greater volume fraction of top layered PCM-1 capsules results into higher thermal storage capacity. The profiles of fluid temperature at outlet of storage tank show that SLSPCM takes 17% 20.5%, 21% less time to charge quicker than CLSPM-1, CLSPM-2 and CLSPCM-3, respectively. This is because hot zone moves downward along the PCM bed due to complete molten state of the top PCMs before the malformation of pinch point interface. And for CLSPCM-1 design, this results into top thin layered PCM-3 facilitating higher energy exchange at a hot operating temperature.

Fig. 7b shows that CLSPCM-3 and SLSPCM has the best and worst thermal performances during the discharge process, respectively. CLSPCM-3 design has a longer discharging period of 193 min followed by CLSPCM-2, CLSPCM-1, SLSPCM with 188 min, 168 min and 152 min, respectively. These results indicate that the use of cascaded layered PCM between SRS help to enhance the energy/exergy output, making use of top and bottom PCMs solidification temperature with the influence of PCM layer thicknesses. However, this effect is more significant for CLSPCM-3 design due to the subsequent release of fluid around the phase transition temperature of the PCMs (PCM-1) which are placed at upper sections of the tank. Moreover, it can be seen that during the same discharging

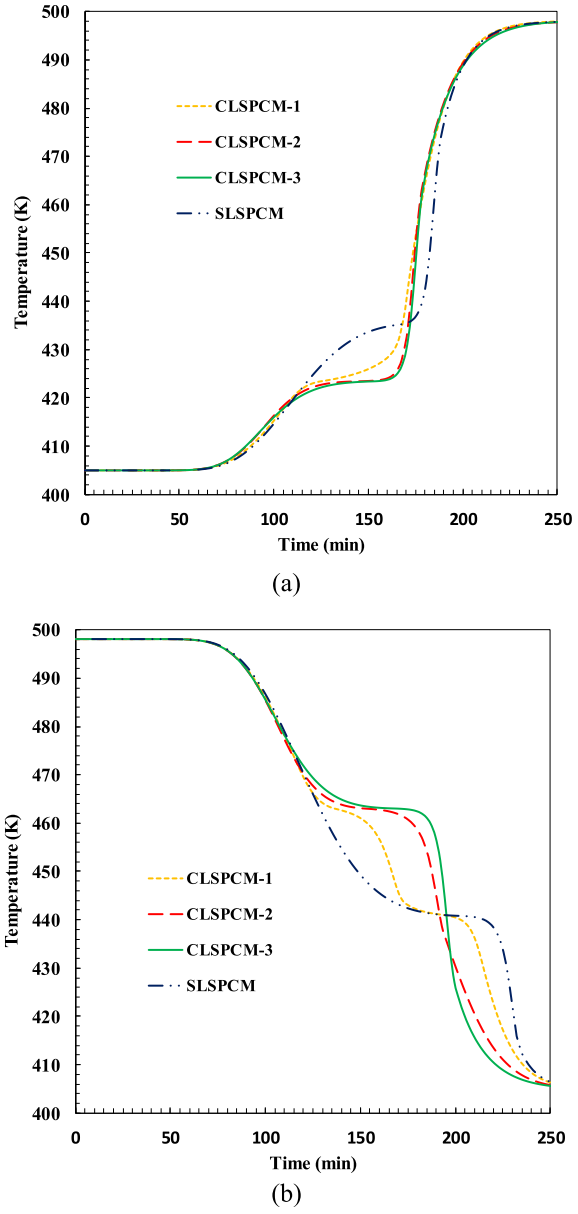

Fig. 7. Temperature of fluid at the outlet as a function of time during (a)charge (b) discharge process.

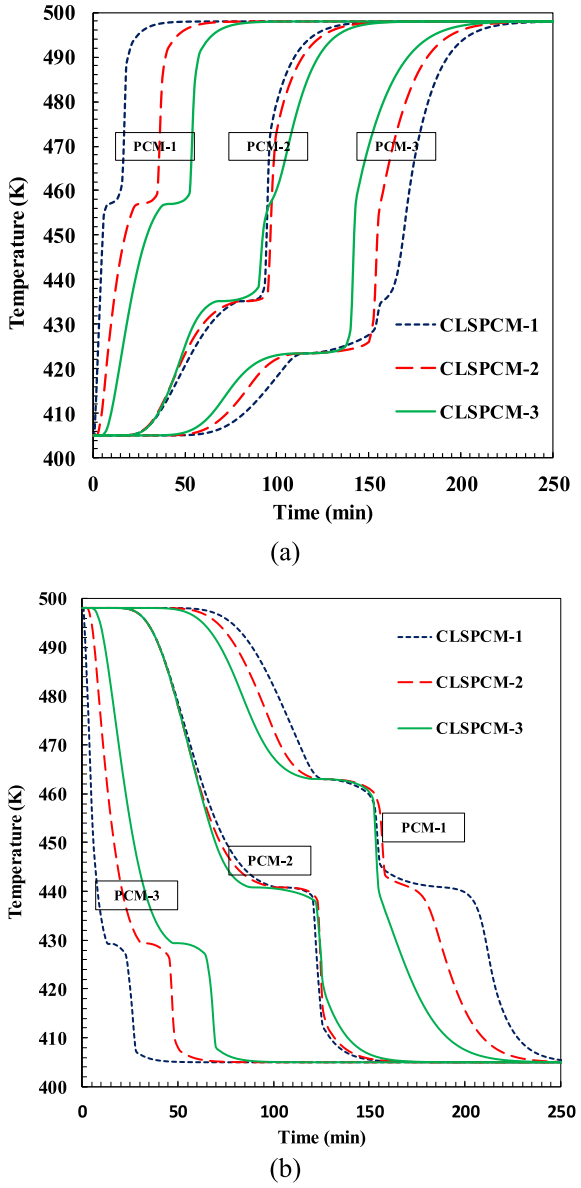

Fig. 8. Variation of temperature profiles at the center of PCM capsules which are placed at mid of each layer thickness during (a)charge (b) discharge process.

time the CLSPCM configurations release HTF in higher exergy state as compared to SLSPCM configuration. Therefore, these results show that the proposed cascaded layered solid PCMs design exhibit a consistent performance both during charging and discharging process.

In order to understand and evaluate the effect of variable volume fractions of PCMs in the descending order of their melting points from top to the bottom of tank, it is important to analyze the variation of temperature profiles in each PCM layer thicknesses. Fig. 8 shows the temporal variation of temperature profiles at the center of PCM capsules for the considered four designed configurations. These PCM capsules are located at the mid of each layer thickness during charge/discharge process. For CLSPCM-1 the center positions of PCM-1, PCM-2 and PCM-3 along tank height are located at 0.3 m, 3 m and 5.7 m respectively. And for CLSPCM-2 the center positions of PCM-1, PCM-2 and PCM-3 are situated at 0.76 m, 3 m and 5.26 m respectively. Similarly, for CLSPCM-3 the center positions of PCM-1, PCM-2 and PCM-3 are located at 1.2 m, 3 m and 4.8 m respectively. The rate of melting or solidification of PCM capsules depends upon the position of phase changing capsule along the tank height in each of the proposed configuration. Their effect on the rate of charge or discharge is represented by the slope of the curve. The steeper the slope the better the dynamic performance of TES system. Fig. 8a shows that PCM-1 capsule for CLSPCM-1 takes only 9 min to change it into molten state, followed by CLSPCM-2 and CLSPCM-3 with 25 min and 39 min, respectively. This is because lower heat of fusion is required for small PCM layer thickness, which accelerates the phase transition process. It makes quick progression of high heated HTF for the coming PCM-2 and PCM-3 layers of capsules. As can be seen that PCM-3 which lies at x = 5.7 m in case of CLSPCM-1; takes longer time for phase transition because it is 7.7% and 15.7% more near to the outlet than in case of CLSPCM-2 and CLSPCM-3, respectively. But it possesses lower exergy values, while PCM-3 for CLSPCM-3 exhibit highest exergy potential and results into higher overall storage capacity.

The same reasoning can be used to explain the solidification process in three layered PCM capsules during the discharge process as shown in Fig. 8b. The results show that PCM-3 capsule has lower thermocline temperature profiles for CLSPCM-3, followed by CLSPCM-2 and CLSPCM-1. This can be attributed to the reason that the higher temperature difference between the HTF and the PCMs in preceding sections of the tank results into greater heat driving force. But later on greater percentage volume fraction of the remaining PCM-3 capsules provide overall higher potential of energy extraction for CLSPCM-3 and CLSPCM-2 than CLSPCM-1.

In order to evaluate the overall performance of a TES unit, it is critical to analyze the effects of comparative temperature distribution of storage filler material i.e., PCM and SRS, on thermocline profiles of HTF. Fig. 9 shows comparative temperature distribution of PCM, SRS and HTF at x = 0.75H as a function of time during charge and discharge process. During the charge process as can be seen in Fig. 9a, the general trend of temperature profiles for all the configurations except CLSPCM-3 show that there is a phase transition around 438 K. This is because these design configurations contain PCM-2 capsules at 4.5 m from the inlet section of tank. Whereas, CLSPCM-3 contains PCM-3 capsules at the same location and is a part of 40% volume fraction of the whole PCM layer thickness. This causes quick phase transition of the PCM capsules around 426 K at 127 min compared to the other configurations. Moreover, it can also be observed from zoomed part of the graph that PCM temperature profiles are at higher exergy states than that of SRS, fluid respectively and it tries to keep the HTF close to its melting point.

Fig. 9b shows that the thermocline layer thickness keeps on expanding as the discharge period proceeds and the temperature reduction of SRS and HTF is high until PCM arrives at its phase transition temperature i.e., 438 K for CLSPCM-2, CLSPCM-1 and SLSPCM. Here the layer of PCM-2 acts as a thermal buffer for HTF and the cold inlet fluid exchanges heat energy with the storage material (SRS and PCMs), while the PCM capsules try to keep the temperature close to its melting point. Hereafter, during phase transition the reduction in fluid temperature is very minor or ignorable over the discharge period as long as PCM keeps on releasing its latent heat and the liquid fraction in PCM starts to decrease. The results show that, for all the configuration cases once the PCM capsule is completely solidified, the temperature profiles of SRS are at higher value than that of phase change material. This is due to the release of only sensible heat by PCMs. It is also noted that the temperature difference between HTF and PCM profiles becomes smaller after phase transition as charge/discharge process proceeds. Therefore, the overall temperature distribution of combined sensible-latent heat TES system show that during discharging when the cold fluid enters through the bottom and the temperature gradient moves to the top section of tank; the layers of low melting point PCM capsules placed near the outlet section remain still in molten state and act as a thermal stabilizer for the outgoing HTF. However, the melting point of PCMs along the layer thicknesses and SRS filler material, affects its thermal gradient at every instant. Phase change material tries to keep the fluid temperature close to its melting point until majority of the PCM near the outlet has solidified. Since the temperature remains within admissible range, the process continuous and the rest of the upstream filler material can be effectively thermally discharged. It allows comparatively longer discharge time and higher thermal energy filling of the whole storage tank. The same effect is also illustrated in Table 4, where the fractions of energy retained after a discharging period of 150 min is evaluated for SRS, PCM and fluid inside the storage tank relative to the total thermal energy.

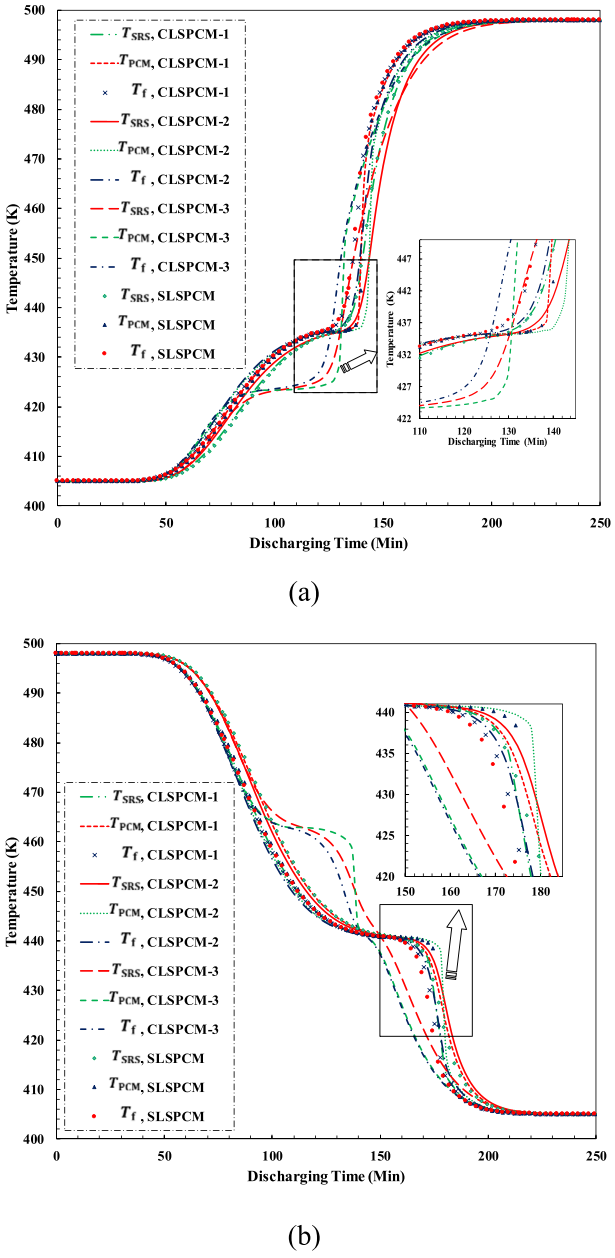

Fig. 9. Comparative temperature variation of PCM, SRS and HTF in TES tank during (a) charging (b) discharging.

3.2. Performance parameters of TES systems

The capacity of TES systems in terms of total amount of energy transferred during charge process and the amount of energy recovered from the tank during discharge process for the proposed TES designs are shown in Fig. 10a and Fig. 10b, respectively. The amount of energy transferred or extracted by the HTF from storage material during charge/discharge cycles is limited by the cutoff temperatures within admissible temperature range of 430 K and 448 K, respectively. The graph shows that the CLSPCM-3 attains the highest performance, CLSPCM-2 the second, CLSPCM-1 the third and SLSPCM is lowest in the row. The CLSPCM-3 design exhibits the superior performance because it possesses the best matching layer thickness and melting temperature distribution of the PCM capsules with the temperature profiles of HTF. Also because the greater

Table 4
Fractions of energy retained relative to total thermal energy after a discharging period of t = 150 min.

Configuration	Energy fraction of PCM (f_{PCM}), %	Energy fraction of SRS (f_{SRS}), %	Energy fraction of Fluid (f_f), %
CLSPCM-1	59	32	9
CLSPCM-2	63	29	8
CLSPCM-3	66	28	6
SLSPCM	58	31	11

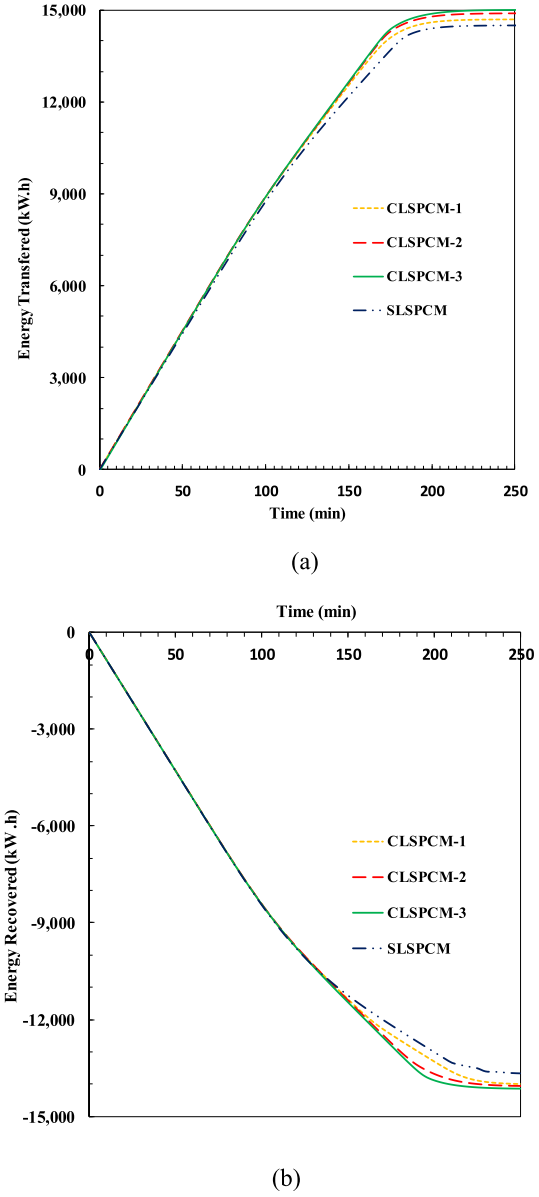

Fig. 10. Total energy (a) transferred during charging (b) recovered during discharging as a function of time.

volume percentage of PCM-1 results into higher storage potential and then this high value of storage capacity is exploited by multi-layered arranged PCM capsules within the admissible temperature range. SLSPCM shows the reduced charge/discharge thermal performance due to the low heat transfer rate between PCM-2 filler and the HTF. SLSPCM is discharged quickly after152 min. Whereas, CLSPCM-1 and CLSPCM-2 deliver the useful energy in 168 min and 188 min, respectively. Whereas, CLSPCM-3 exhibit the highest discharging period of 193 min. Moreover, it is noted that the low melting point PCM-3 at the end section of tank serves as a buffer to maintain the saturation conditions, allowing the TES unit to discharge for longer duration and recover greater heat energy at higher exergy state.

Fig. 11 shows comparative thermal performance results in terms of charging, discharging efficiency and overall efficiency. CLSPCM-3 design attains the highest overall efficiency of 80%, followed by CLSPCM-2, CLSPCM-1 and SLSPCM exhibiting 78%, 72% and 65%, respectively. This is attributed to the reason that each of the PCM-3 and PCM-1 layers placed at the lateral sections of tank, take the advantage of incoming high exergy fluid flow which help to accelerate phase transition process at the pinch point interfaces of the proceeding capsules. This results in to enhanced utilization of latent heat energy as well as extraction of sensible heat from SRS. For CLSPCM-1, the higher volume fraction i.e., 40% of top PCM-1 during charging process takes longer time to break the pinch point interface. However, the higher temperature difference between the preceding PCMs melting point and the hot inlet fluid stimulates a bigger heat driving force. This promotes quick progression of the PCM interface. Moreover, the high percentage layers of low melting point PCM-3 capsules placed near the outlet section remain in liquid state for longer time and act as thermal stabilizer for the outgoing HTF. This results into enhanced potential of energy extraction and improved overall energy efficiency for CLSPCM-3 as compared to CLSPCM-2 and CLSPCM-1, respectively. Moreover, SLSPCM shows the least overall energy efficiency because of low heat transfer rate between single layered PCM-2 and HTF. It causes lower extraction of latent heat and some part of the thermal energy remains unused due to the solidification.

Additional performance indices of the investigated TES designs are enlisted in Table 5. CLSPCM-3 and SLSPCM show the best and

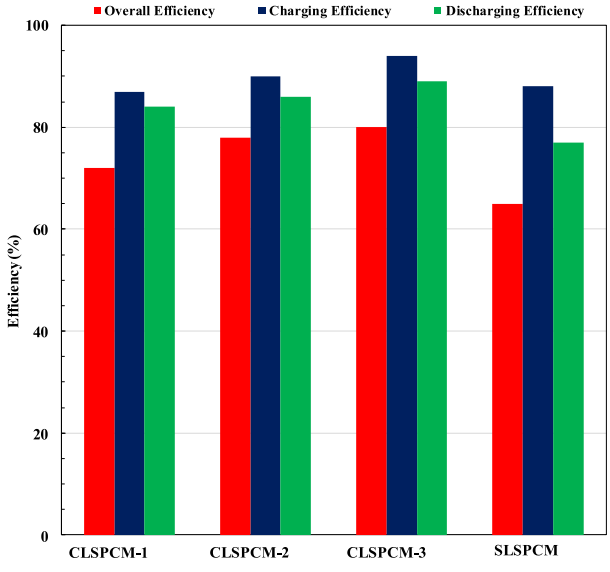

Fig. 11. Performance parameters for the considered four different configurations.

Table 5
Performance indices of the four different configurations.

Performance Parameter	SLSPCM	CLSPCM-1	CLSPCM-2	CLSPCM-3
Effective discharging time (min)	152	168	188	193
Utilization ratio	0.49	0.55	0.65	0.74
Capacity ratio	0.59	0.61	0.68	0.75
Exergy efficiency (%)	58	64	73	78
Storage capacity (kWhr/m^3)	123.8	126.4	135.3	140.1
Pump energy/Stored energy (%)	0.06	0.06	0.06	0.06

the lowest exergy efficiency of 78% and 58%, respectively. The pumping energy required to overcome the pressure drop in TES system is less than 0.061% for all the considered configurations. The higher utilization ratio of 0.74 for CLSPCM-3 case indicates that high and low melting point PCMs placed at the lateral sections of tank act as thermal "buffer" for the outgoing HTF. It tries to keep the fluid temperature close to the melting point until majority of the PCM near outlet has solidified, resulting into enhanced exergy efficiencies. Moreover, in Table 5 the value of storage capacity per unit volume indicates that the thermal performance of TES configurations is very much influenced by this factor. High volume percentage (40%) of PCM-1 layer in the upper section of storage tank for CLSPCM-3 results into 3.5% and 9.5% higher storage capacity (kWhr/m^3) value than that of CLSPCM-2 and CLSPCM-1, respectively. Whereas, SLSPM exhibit the least storage capacity of 123.8 kWhr/m^3. This is because of relatively greater thickness of PCM-1 layer and higher storage density. Higher storage capacity value means more thermal energy is available to be recovered during discharging period and hence this results into longer discharging time with enhanced overall efficiency.

4. Conclusions

In the current study, transient, two-phase Schumann model equations are evaluated numerically to investigate the influence of combined sensible-latent heat storage material on thermocline characterization. The main idea of the current work is to fill a thermocline TES tank with cascaded PCM capsules comprising of different volume fractions in such a way that majority of it can effectively undergo the phase change and together with the inclusion of sensible heat cheaper structured material; offering a much more efficient and cost-effective thermal storage alternative. The main findings from the current work are summarized follows;

(1) An optimized cascaded design of multilayered PCMs with suitable combination of melting point and layer thickness in between sensible heat structure material, is a critical aspect in defining the overall performance of a single TES unit.
(2) The selection of PCMs within admissible temperature range placed at the lateral ends of storage tank must be made carefully. As these layers with decreasing melting points and variable thicknesses must take the advantage of incoming high exergy fluid flow to accelerate the phase transition process at the pinch point interfaces of PCM capsules during charge/discharge cycles. This enhances the utilization of latent heat energy as well as extraction of sensible heat from SRS.
(3) CLSPCM-3 design offers considerably improved charge/discharge thermal performance than the other three considered prototypes. This is because the temperature profiles of HTF matched well with the cascaded PCM layer thicknesses and the melting point variations along the tank height within admissible temperature range.
(4) The lower utilization ratio of 0.49 for SLSPCM configuration indicates that the PCMs at the bottom of the tank are not melted completely and the highest temperature achieved for the single layered PCM is much lower than that of CLSPCM-3 exhibiting the utilization ratio of 0.74. This is because of the buffer effect of PCM capsules placed at the lateral sections of storage tank. These try to keep fluid temperature close to the melting point until majority of the PCM near outlet has solidified, resulting into enhanced exergy efficiencies.
(5) CLSPCM-3 attains the highest overall efficiency of 80% followed by SLSPCM-2, SLSPCM-1 having 78%, 72%, respectively and SLSPCM is last in the row with 65%. CLSPCM-3 and SLSPCM show the highest and the lowest exergy efficiencies of 78% and 58%, respectively.

The design analysis presented in the current work shows that for CLSPCM configurations, the correct arrangement design of PCM layers with suitable fusion temperature and volume fraction in between structured rod is a critical aspect in determining the final performance of the TES system.

Author contribution statement

N. Ahmed: Conceptualization, Methodology, Investigation. Writing- Original draft preparation. **K.E. Elfeky**: Software, Validation. **Lin LU**: Writing- Reviewing and Editing. **Q.W. Wang**: Supervision, Writing- Reviewing and Editing.

Declaration of competing interest

The authors declare that they have no known competing financial interests or personal relationships that could have appeared to influence the work reported in this paper.

Acknowledgments

This work is financially supported by the National Natural Science Foundation of China (Grant No. 51536007), the National Natural Science Foundation of China (NSFC)/Research Grants Council (RGC) Joint Research Scheme (Grant No. 51861165105), the Foundation for Innovative Research Groups of the National Natural Science Foundation of China (Grant No. 51721004) and the 111 Project (Grant No. B16038).

References

[1] Ş. Kılkış, G. Krajačić, N. Duić, M.A. Rosen, M.A. Al-Nimr, Advancements in sustainable development of energy, water and environment systems, Energy Convers. Manag. 176 (2018) 164–183, https://doi.org/10.1016/j.enconman.2018.09.015.
[2] M. Jiménez-Arreola, R. Pili, F. Dal Magro, C. Wieland, S. Rajoo, A. Romagnoli, Thermal power fluctuations in waste heat to power systems: an overview on the challenges and current solutions, Appl. Therm. Eng. 134 (2018) 576–584, https://doi.org/10.1016/j.applthermaleng.2018.02.033.
[3] U. Pelay, L. Luo, Y. Fan, D. Stitou, M. Rood, Thermal energy storage systems for concentrated solar power plants, Renew. Sustain. Energy Rev. 79 (2017) 82–100, https://doi.org/10.1016/j.rser.2017.03.139.
[4] A.G. Olabi, Renewable energy and energy storage systems, Energy 136 (2017) 1–6, https://doi.org/10.1016/j.energy.2017.07.054.
[5] C. Libby, Solar Thermocline Storage Systems: Preliminary Design Study, Electr. Power Res. Institute, Palo Alto, CA, 2010.
[6] L.J. Shah, S. Furbo, Entrance effects in solar storage tanks, Sol. Energy 75 (2003) 337–348, https://doi.org/10.1016/j.solener.2003.04.002.
[7] S.M. Flueckiger, Z. Yang, S. V Garimella, Review of molten-salt thermocline tank modeling for solar thermal energy storage, Heat Tran. Eng. 34 (2013) 787–800.
[8] Lazard, Lazard's levelised cost of storage v2.0, Clim. Pol. 6 (2016) 600–606, https://doi.org/10.1080/14693062.2006.9685626.
[9] Y. Jemmal, N. Zari, M. Maaroufi, Thermophysical and chemical analysis of gneiss rock as low cost candidate material for thermal energy storage in concentrated solar power plants, Sol. Energy Mater. Sol. Cells 157 (2016)

377–382, https://doi.org/10.1016/j.solmat.2016.06.002.
[10] G. Alva, L. Liu, X. Huang, G. Fang, Thermal energy storage materials and systems for solar energy applications, Renew. Sustain. Energy Rev. 68 (2017) 693–706, https://doi.org/10.1016/j.rser.2016.10.021.
[11] J. Pereira da Cunha, P. Eames, Thermal energy storage for low and medium temperature applications using phase change materials – a review, Appl. Energy 177 (2016) 227–238, https://doi.org/10.1016/j.apenergy.2016.05.097.
[12] P. Abhiji, L. Shi, C.W. Bielawski, A eutectic mixture of galactitol and mannitol as a phase change material for latent heat storage, Energy Convers. Manag. 103 (2015) 139–146, https://doi.org/10.1016/j.enconman.2015.06.013.
[13] R.P. Singh, S.C. Kaushik, D. Rakshit, Melting phenomena in a finned thermal storage system with graphene nano-plates for medium temperature applications, Energy Convers. Manag. 163 (2018) 86–99, https://doi.org/10.1016/j.enconman.2018.02.053.
[14] H. Ettouney, H. El-Dessouky, A. Al-Ali, Heat transfer during phase change of paraffin wax stored in spherical shells, J. Sol. Energy Eng. 127 (2005) 357, https://doi.org/10.1115/1.1850487.
[15] N. Nallusamy, S. Sampath, R. Velraj, Experimental investigation on a combined sensible and latent heat storage system integrated with constant/varying (solar) heat sources, Renew. Energy 32 (2007) 1206–1227, https://doi.org/10.1016/j.renene.2006.04.015.
[16] J.P. Kotzé, T.W. Von Backström, P.J. Erens, Simulation and testing of a latent heat thermal energy storage unit with metallic phase change material, Energy Procedia 49 (2013) 860–869, https://doi.org/10.1016/j.egypro.2014.03.093.
[17] S.M. Flueckiger, S.V. Garimella, Latent heat augmentation of thermocline energy storage for concentrating solar power - a system-level assessment, Appl. Energy 116 (2014) 278–287, https://doi.org/10.1016/j.apenergy.2013.11.059.
[18] T.K. Aldoss, M.M. Rahman, Comparison between the single-PCM and multi-PCM thermal energy storage design, Energy Convers. Manag. 83 (2014) 79–87, https://doi.org/10.1016/j.enconman.2014.03.047.
[19] B. chen Zhao, M. song Cheng, C. Liu, Z. min Dai, Thermal performance and cost analysis of a multi-layered solid-PCM thermocline thermal energy storage for CSP tower plants, Appl. Energy 178 (2016) 784–799, https://doi.org/10.1016/j.apenergy.2016.06.034.
[20] K.E. Elfeky, N. Ahmed, Q. Wang, Numerical comparison between single PCM and multi-stage PCM based high temperature thermal energy storage for CSP tower plants, Appl. Therm. Eng. 139 (2018) 609–622, https://doi.org/10.1016/j.applthermaleng.2018.04.122.
[21] S.M. Flueckiger, Z. Yang, S.V. Garimella, Thermomechanical simulation of the solar one thermocline storage tank, J. Sol. Energy Eng. 134 (2012), 041014, https://doi.org/10.1115/1.4007665.
[22] M.N. Strasser, R.P. Selvam, A cost and performance comparison of packed bed and structured thermocline thermal energy storage systems, Sol. Energy 108 (2014) 390–402, https://doi.org/10.1016/j.solener.2014.07.023.
[23] M. Abarr, B. Geels, J. Hertzberg, L.D. Montoya, Pumped thermal energy storage and bottoming system part A: concept and model, Energy 120 (2017) 320–331, https://doi.org/10.1016/j.energy.2016.11.089.
[24] Q.W.W.N. Ahmed, K.E. Elfeky, Mumtaz A. Qaisrani, Numerical characterization of thermocline behaviour of combined sensible-latent heat storage tank using brick manganese rod structure impregnated with PCM capsules, Sol. Energy (2019).
[25] G. Zanganeh, M. Commerford, A. Haselbacher, A. Pedretti, A. Steinfeld, Stabilization of the outflow temperature of a packed-bed thermal energy storage by combining rocks with phase change materials, Appl. Therm. Eng. 70 (2014) 316–320, https://doi.org/10.1016/j.applthermaleng.2014.05.020.
[26] P.A. Galione, C.D. Perez-Segarra, I. Rodriguez, A. Oliva, J. Rigola, Multi-layered solid-PCM thermocline thermal storage concept for CSP plants. Numerical analysis and perspectives, Appl. Energy 142 (2015) 337–351, https://doi.org/10.1016/j.apenergy.2014.12.084.
[27] N. Ahmed, K.E. Elfeky, Q. Wang, Comparative thermo-economic analysis of structured thermocline combined sensible-latent heat thermal energy storage systems for medium temperature applications, in: 13th Conf. Proc. SDEWES2018.0255, 2018.
[28] N. Ahmed, K.E. Elfeky, L. Lu, Q.W. Wang, Thermal and economic evaluation of thermocline combined sensible-latent heat thermal energy storage system for medium temperature applications ☆, Energy Convers. Manag. 189 (2019) 14–23, https://doi.org/10.1016/j.enconman.2019.03.040.
[29] A. Crespo, C. Barreneche, M. Ibarra, W. Platzer, Latent thermal energy storage for solar process heat applications at medium-high temperatures – a review, Sol. Energy (2018), https://doi.org/10.1016/J.SOLENER.2018.06.101.
[30] D.D.I. Ricerca, Modelling , Design and Analysis of Innovative Thermal Energy Storage Systems Using PCM for Industrial Processes , Heat and Power, 2015.
[31] H. Nazir, M. Batool, F.J. Bolivar Osorio, M. Isaza-Ruiz, X. Xu, K. Vignarooban, P. Phelan, Inamuddin, A.M. Kannan, Recent developments in phase change materials for energy storage applications: a review, Int. J. Heat Mass Tran. 129 (2019) 491–523, https://doi.org/10.1016/J.IJHEATMASSTRANSFER.2018.09.126.
[32] G. John, A. Ko, C.K. King, D. Bru, ScienceDirect Galactitol as Phase Change Material for Latent Heat Storage of Solar Cookers : Investigating Thermal Behavior in Bulk Cycling, vol. 119, 2015, pp. 415–421, https://doi.org/10.1016/j.solener.2015.07.003.
[33] J.T. Van Lew, P. Li, C.L. Chan, W. Karaki, J. Stephens, Analysis of heat storage and delivery of a thermocline tank having solid filler material, J. Sol. Energy Eng. 133 (2011), 021003, https://doi.org/10.1115/1.4003685.
[34] L.V. Kim, Determination of the heat transfer coefficients in porous media, J. Eng. Phys. Thermophys. 65 (1993) 1168–1172, https://doi.org/10.1007/BF00861937.
[35] N. Wakao, S. Kaguei, T. Funazkri, Effect of fluid dispersion coefficients on particle-to-fluid heat transfer coefficients in packed beds. Correlation of nusselt numbers, Chem. Eng. Sci. 34 (1979) 325–336, https://doi.org/10.1016/0009-2509(79)85064-2.
[36] A. Felix Regin, S.C. Solanki, J.S. Saini, An analysis of a packed bed latent heat thermal energy storage system using PCM capsules: numerical investigation, Renew. Energy 34 (2009) 1765–1773, https://doi.org/10.1016/j.renene.2008.12.012.
[37] P. Chandra, D.H. Willits, Pressure drop and heat transfer characteristics of air-rockbed thermal storage systems, Sol. Energy 27 (1981) 547–553, https://doi.org/10.1016/0038-092X(81)90050-5.
[38] M. Hänchen, S. Brückner, A. Steinfeld, High-temperature thermal storage using a packed bed of rocks - heat transfer analysis and experimental validation, Appl. Therm. Eng. 31 (2011) 1798–1806, https://doi.org/10.1016/j.applthermaleng.2010.10.034.
[39] K. Nithyanandam, R. Pitchumani, A. Mathur, Analysis of a latent thermocline storage system with encapsulated phase change materials for concentrating solar power, Appl. Energy 113 (2014) 1446–1460, https://doi.org/10.1016/j.apenergy.2013.08.053.
[40] S. Kuravi, J. Trahan, Y. Goswami, C. Jotshi, E. Stefanakos, N. Goel, Investigation of a high-temperature packed-bed sensible heat thermal energy storage system with large-sized elements, J. Sol. Energy Eng. 135 (2013), 041008, https://doi.org/10.1115/1.4023969.